Journal of Physics: Conference Series **498** (2014) 012004 doi:10.1088/1742-6596/498/1/012004

HIFU scattering by the ribs: constrained optimisation with a complex surface impedance boundary condition

P Gélat[1,2,†], G ter Haar[3] and N Saffari[2]

[1] National Physical Laboratory, Hampton Road, Teddington TW11 0LW, United Kingdom.
[2] Department of Mechanical Engineering, University College London, Torrington Place, London WC1E 7JE, United Kingdom.
[3] Therapeutic Ultrasound Group, Joint Physics Department, Institute of Cancer Research, Sutton SM2 5NG, United Kingdom.

[†] E-mail: Pierre.Gelat@npl.co.uk

Abstract. High intensity focused ultrasound (HIFU) enables highly localised, non-invasive tissue ablation and its efficacy has been demonstrated in the treatment of a range of cancers, including those of the kidney, prostate and breast. HIFU offers the ability to treat deep-seated tumours locally, and potentially bears fewer side effects than more established treatment modalities such as resection, chemotherapy and ionising radiation. There remains however a number of significant challenges which currently hinder its widespread clinical application. One of these challenges is the need to transmit sufficient energy through the ribcage to ablate tissue at the required foci whilst minimising the formation of side lobes and sparing healthy tissue. Ribs both absorb and reflect ultrasound strongly. This sometimes results in overheating of bone and overlying tissue during treatment, leading to skin burns. Successful treatment of a patient with tumours in the upper abdomen therefore requires a thorough understanding of the way acoustic and thermal energy is deposited. Previously, a boundary element (BE) approach based on a Generalised Minimal Residual (GMRES) implementation of the Burton-Miller formulation was developed to predict the field of a multi-element HIFU array scattered by human ribs, the topology of which was obtained from CT scan data [1]. Dissipative mechanisms inside the propagating medium have since been implemented, together with a complex surface impedance condition at the surface of the ribs. A reformulation of the boundary element equations as a constrained optimisation problem was carried out to determine the complex surface velocities of a multi-element HIFU array which generated the acoustic pressure field that best fitted a required acoustic pressure distribution in a least-squares sense. This was done whilst ensuring that an acoustic dose rate parameter at the surface of the ribs was kept below a specified threshold. The methodology was tested at an excitation frequency of 1 MHz on a spherical multi-element array in the presence of anatomical ribs.

1. Background

High intensity focused ultrasound (HIFU) enables highly localised, non-invasive tissue ablation and its efficacy has been demonstrated for treating a range of cancers, including abdominal tumours [2], [3].

One of the challenges of trans-rib high-intensity focused ultrasound treatment is the need to transmit sufficient energy through the ribcage to ablate tissue whilst minimising the formation of side lobes, and sparing healthy tissue. Ribs strongly absorb and reflect ultrasound. This may result in

overheating of bone and overlying tissue during treatment, leading to skin burns [3], [4], [5]. Hence, care must be taken so that sufficient energy is delivered through the rib cage ensuring that acoustic pressures at the treatment location are above the ablation threshold at the focus while at the same time maintaining the formation of side lobes to a minimal level. Approaches using multi-element piezoelectric transducer arrays in conjunction with multi-channel electronics have been suggested, where the magnitude and phase of each transducer element may be adjusted to help minimise acoustic pressures on the ribs. Commonly, pre-operative treatment planning strategies using such phased arrays rely on the deactivation of transducer elements obstructed by ribs, or so-called binarised apodisation [6], [7], [8]. Whilst this approach is convenient in its implementation, deactivation of elements will significantly reduce the ultrasonic power delivered at the focus and an increase in treatment time may occur as a result. Furthermore, it does not attempt to address the inverse problem of optimising the magnitudes and phases of the transducer element drive voltage in order to induce tissue necrosis at the required foci, whilst keeping the pressure on the ribs below a chosen threshold, and ensuring minimal formation of side-lobes.

Some of the limitations of binarised apodisation can be addressed in an approach based on the decomposition of the time reversal operator (DORT) [9]. The application of the DORT method to focusing through the ribs has been discussed by Cochard *et al* in 3D [10]. Using a singular value decomposition of the inter-element array response matrix, an excitation weight vector is obtained which is orthogonal to the subspace of emissions focusing on the rib. When applied to the array, this excitation vector enhances the acoustic energies deposited at the focal point compared with those on the ribs. Furthermore, Ballard *et al* proposed an experimentally validated method of an adaptive, image-based refocusing algorithm of dual-mode ultrasound arrays in the presence of scatterers [11]. This approach and the DORT method both have the advantage of not requiring *a priori* knowledge of the location of the ribs. Nevertheless, neither method directly quantifies energy depositions on the surface of the ribs, both relying instead on information from the back-scattered signal.

The inverse problem of focusing the field of a multi-element HIFU array inside the rib cage whilst ensuring that the pressure magnitude on the surface of the ribs does not exceed a given damage threshold, was addressed by Gélat *et al* [12]. The forward model employed a boundary element approach in which it was possible to address the effects of scattering and diffraction on 3D anatomical data [1]. In both these studies, the ribs modelled as perfectly rigid scatterers: this simplification is somewhat limiting as, although rib bone does indeed possess much higher impedance than soft tissue, ribs are not perfect reflectors.

Although there is no universally recognized meaning ‘acoustic dose’, in the context of this paper acoustic dose rate is defined as the time-averaged rate of heat generation by relaxational absorption per unit volume, following Duck [13]. Under continuous wave conditions and for linear wave propagation, this quantity $\langle q_v \rangle$ may be expressed as follows [14],

$$\langle q_v \rangle = \alpha \frac{|p|^2}{\rho c} \tag{1}$$

where

- α is the absorption coefficient arising from relaxation mechanisms when the shear viscosity is set to zero
- $|p|$ is the acoustic pressure magnitude
- ρ is the medium density
- c is the velocity of sound

The brackets $\langle \quad \rangle$ denote a temporal average. These will be omitted in the remainder of this paper and the acoustic dose rate will be referred to as q_v.

In this study, the boundary element approach described in [1] and [12] was extended to incorporate an acoustic impedance boundary condition on the surface of the scatterer. This implementation was validated against an analytical solution for the scattering of a plane wave by a non-rigid sphere. Calculations using the forward model were then carried out on a rib mesh obtained from anatomical

data. The acoustic source was 256-element spherical array with a pseudo-random distribution of elements on its surface. The inverse problem was solved using the same approach as in [12]. Using a Numerical Algorithms Group (NAG) Numerical Library routine [15], which calculates the minimum of a sum of squares for a set of nonlinear constraints, optimal values for the real and imaginary parts of the element velocities were obtained so that the acoustic pressures at specified locations in the exterior domain best fitted a required field distribution in a least-squares sense. Implementation of the constraints ensured that the acoustic dose rate on the surface of the ribs did not exceed a specified threshold and that the element velocity magnitudes were kept within the specified dynamic range.

2. Theory

Consider a scatterer defined by a closed smooth surface *S*. Let the medium surrounding the scatterer be defined as the exterior domain V_{ext}. Let the boundary condition at infinity satisfy Sommerfeld's acoustic radiation condition. The propagation of time-harmonic acoustic waves in a homogeneous isotropic inviscid medium is described by the Helmholtz equation:

$$\nabla^2 p(\vec{r}) + k^{*2} p(\vec{r}) = 0, \forall \vec{r} \in V_{ext} \tag{2}$$

where p is the acoustic pressure, $k^* = \omega / c^*$ is the acoustic wave number where ω is the angular frequency, c^* the complex sound speed in the external medium and $\vec{r}$ is the position vector. A source term may be included in the right hand side of (2) (incident pressure wave), but it is convenient to split the total pressure $p(\vec{r})$ as the sum of the incident pressure $p_i(\vec{r})$ and the pressure scattered by the surface *S*, $\forall \vec{r} \in V_{ext}$.

For scattering problems, the integral representation of the solution to (2) is given by the Helmholtz integral equation [16]:

$$\int_S \left[p(\vec{r}_q) \frac{\partial G(\vec{r}|\vec{r}_q)}{\partial n_q} - \frac{\partial p(\vec{r}_q)}{\partial n_q} G(\vec{r}|\vec{r}_q) \right] dS = \frac{1}{2} p(\vec{r}) - p_i(\vec{r}), \forall \vec{r} \in S \tag{3}$$

$$\int_S \left[p(\vec{r}_q) \frac{\partial G(\vec{r}|\vec{r}_q)}{\partial n_q} - \frac{\partial p(\vec{r}_q)}{\partial n_q} G(\vec{r}|\vec{r}_q) \right] dS = p(\vec{r}) - p_i(\vec{r}), \forall \vec{r} \in V_{ext} \tag{4}$$

where the Green's function in a three-dimensional space is given by:

$$G(\vec{r}|\vec{r}_q) = \frac{1}{4\pi \|\vec{r} - \vec{r}_q\|} e^{-ik^* \|\vec{r} - \vec{r}_q\|} \tag{5}$$

and $p(\vec{r}_q)$ is the pressure on the surface *S* at point $\vec{r}_q$ and $\vec{n}_q$ is the outward normal.

By using the linearised conservation of momentum equation on *S*, and by noting that ratio of the acoustic pressure and the normal component of the particle velocity vector on *S* is equal to the characteristic acoustic impedance of the scatterer, equations (3) and (4) may be rewritten as follows.

$$\int_S \left[p(\vec{r}_q) \frac{\partial G(\vec{r}|\vec{r}_q)}{\partial n_q} + ik^* \frac{\rho c^*}{\rho_1 c_1} p(\vec{r}_q) G(\vec{r}|\vec{r}_q) \right] dS = \frac{1}{2} p(\vec{r}) - p_i(\vec{r}), \forall \vec{r} \in S \tag{6}$$

$$\int_S \left[p(\vec{r}_q) \frac{\partial G(\vec{r}|\vec{r}_q)}{\partial n_q} + ik^* \frac{\rho c^*}{\rho_1 c_1} p(\vec{r}_q) G(\vec{r}|\vec{r}_q) \right] dS = p(\vec{r}) - p_i(\vec{r}), \forall \vec{r} \in V_{ext} \tag{7}$$

where

- ρ is the density of the acoustic medium in the exterior domain
- ρ_1 is the density of the scatterer
- c_1 is the speed of sound associated with the scatterer.

It is well known that the problem described by the discretisation of integral equation (6) suffers from non-uniqueness at frequencies of excitation approaching an eigenvalue of one of the (fictitious)

modes of the cavity inside the scatterer. After discretising equation (6), the resulting matrix obtained becomes close to singular. For a wave number whose imaginary part is non-zero, solving the discretised form of equation (6) is often be sufficient, as the fictitious modes of the cavity inside the scatterer are likely to be damped out [17]. For the complex sound speed, frequency of excitation and scatterer dimensions considered in this paper, it has shown that a discretisation of the Helmholtz integral equation is indeed sufficient and that the coupling term involving the normal derivative formulation need not be considered [12]. This validation will was repeated as part of this work for a non-rigid spherical scatterer with a complex surface impedance condition. The results are shown in Section 3.

The formulation of the inverse problem is described fully in [12]. It is summarised below. By discretising equation (6), for all position vectors $\vec{r}$ on S corresponding to each node on the mesh of the surface, a linear system of equations may be generated.

$$[H]\{p_{surf}\} = -\{p_i\} \tag{8}$$

where $[H]$ is the boundary element matrix and the acoustic pressures on the surface S have been relabelled $\{p_{surf}\}$. It should be noted that the $[H]$ matrix referred to in this work differs from that in [12] in that it contains the contribution of terms associated with the integration of the normal derivative of the acoustic pressure multiplied by the Green's function over the surface S.

Let the incident acoustic pressure field be a linear combination of plane circular pistons rigidly vibrating in an infinite baffle. The incident field on S may be written as a linear combination of the source velocities of each piston as follows:

$$[H]\{p_{surf}\} = -[\beta]\{U\} \tag{9}$$

where the elements of $[\beta]$ may be obtained analytically in the far-field or by solving the Rayleigh integral in the near-field. $[\beta]$ is of dimension $M\times N$, where M is the number of nodes on the surface S after its discretisation and N is the number of plane pistons. $\{U\}$ is the vector of source velocities and is of dimension $N\times 1$.

Consider equation (6), where the position vectors are located in the exterior volume V_{ext}. For specified number of locations in the exterior volume, we have [12]:

$$[Q]\{p_{surf}\} = \{p_{ext}\} - [\gamma]\{U\} \tag{10}$$

where $[Q]$ is a matrix of weighting coefficients and the acoustic pressures in the exterior volume V_{ext} have been relabelled $\{p_{ext}\}$.

The vector of surface pressures may be eliminated by combining equations (9) and (10).

$$([\gamma] - [Q][H]^{-1}[\beta])\{U\} = \{p_{ext}\} \tag{11}$$

Equation (9) may be re-written as follows.

$$-[H]^{-1}[\beta]\{U\} = \{p_{surf}\} \tag{12}$$

or

$$[A]\{U\} = \{p_{surf}\} \tag{13}$$

where $[A] = -[H]^{-1}[\beta]\{U\}$.

Equations (11) may be re-written as follows.

$$[C]\{U\} = \{p_{ext}\} \tag{14}$$

where $[C] = [\gamma] - [Q][H]^{-1}[\beta]$.

When investigating an inverse problem involving complex quantities, it is convenient to reformulate in terms of purely real variables by rewriting equation (12) as follows:

$$\begin{bmatrix} \mathrm{Re}[C] & -\mathrm{Im}[C] \\ \mathrm{Im}[C] & \mathrm{Re}[C] \end{bmatrix} \begin{Bmatrix} \mathrm{Re}\{U\} \\ \mathrm{Im}\{U\} \end{Bmatrix} = \begin{Bmatrix} \mathrm{Re}\{p_{ext}\} \\ \mathrm{Im}\{p_{ext}\} \end{Bmatrix} \tag{15}$$

or

$$[\hat{C}]\{\hat{U}\} = \{\hat{p}_{ext}\} \tag{16}$$

We wish to obtain a set of real and imaginary parts of source velocities which best fit a prescribed field pressure distribution in a least-squares sense such that:

- the acoustic dose rate on *S* as defined in equation (1) does not exceed a threshold defined by $q_{v_{max}}$
- the source velocity magnitudes do not exceed the upper bound of the dynamic range of each element U_{max}.

This may be expressed as a least-squares minimisation problem with nonlinear constraints:

$$\min_{\hat{U}} \frac{1}{2} \left\| [\hat{C}]\{\hat{U}\} - \{\hat{p}_{ext}\} \right\|_2^2 \text{ such that } \begin{cases} q_v \leq q_{v_{max}} \\ |U| \leq U_{max} \end{cases} \tag{17}$$

The HIFU transducer modelled investigated in this paper was the same as in [12]. It is a spherically shaped bowl populated with $N = 256$ plane circular elements mounted onto its surface. The elements are each of $a = 3$ mm radius and of curvature $D = 18$ cm. The outer diameter of the HIFU transducer is 16 cm. The elements are pseudo-randomly spatially distributed on the surface of the array. The excitation frequency was assumed to be 1 MHz.

The rib topology was obtained from a human cadaver in STereoLithography format. Ribs 9-12 on the right side were truncated from the spine and closed surfaces were fitted over each rib using the Geomagic® software. CATIA v5 Advanced Meshing Tools were used to mesh the surfaces.

Within the context of this work, $q_{v_{max}}$ was chosen as 30% of the maximum value of the acoustic dose rate on the surface of the ribs resulting from all elements vibrating in phase and with 1 m s^{-1} amplitude velocity. This 30% value is not necessarily of clinical significance and was arbitrarily chosen to illustrate the technique. It is understood that in clinical applications, a damage threshold related to this dose rate quantity would have to be experimentally established

3. Results

The Helmholtz integral equation boundary element approach was implemented on a dedicated computer cluster and solved using Generalised Minimal Residual (GMRES) implementation. The approach used here differs from that described in [1] as follows.

- The speed of sound in the exterior domain was specified as a complex number in order to account for an amplitude absorption coefficient in the medium.
- Operations were vectorised to solve equation (6) for multiple right hand sides simultaneously, which enabled the coefficients of [*A*] to be obtained more efficiently.
- The term in the surface Helmholtz integral equation containing the normal derivative of the acoustic pressure was accounted for in order to account for a locally reacting surface with a known specific admittance.

The routines employed to generate the boundary element matrices were obtained from the PAFEC (Program for Automatic Finite Element Calculations) VibroAcoustics software with permission from PACSYS Ltd.

A calculation on a simple scatterer was carried out for validation purposes. The results displayed here are for a 1 MHz unit amplitude plane wave scattered by a sphere with a complex surface impedance condition. The sphere was 10 mm in diameter and centred on the origin. These were

compared against the analytical provided in [18] in the shadow zone between 5.5 mm and 25 mm (see figure 2).

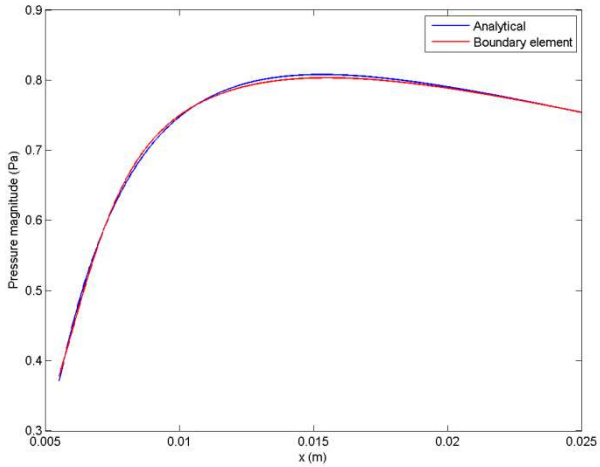

Figure 1. Helmholtz integral equation implementation of BE formulation on a spherical scatterer of 10 mm diameter. Incident field: unit amplitude 1 MHz plane wave travelling in positive x direction. Comparison along the x-axis against analytical solution.

The scatterer was meshed using isoparametric eight-noded quadratic patches ensuring at least three elements per wavelength for a wavespeed of 1500+4.405i m s^{-1}. The density of the medium was assumed to be 1000 kg m^{-3}. The properties of the scatterer were chosen to be representative of rib bone. The density of the scatterer was assumed to be 1912 kg m^{-3} and the speed of sound of longitudinal waves 4080 m s^{-1} [19]. The absorption coefficient of the scatterer was assumed to be 47.2 Np m^{-1} at 1 MHz [20]. Figure 1 shows agreement within 1.8% of the analytical solution on the x-axis in the shadow zone.

After completing this validation, the incident acoustic pressure field was replaced with that of the multi-element array described in [12] and a suitable mesh of the anatomical ribs described in Section 2 was generated. A simulation solving equation (6) for multiple right hand sides was launched so that the product $[H]^{-1}[\beta]$ could be obtained in four separate runs. The global origin was chosen to be at the focus of the array with propagation taking place along the positive z direction. This configuration is illustrated in plan view in figure 2.

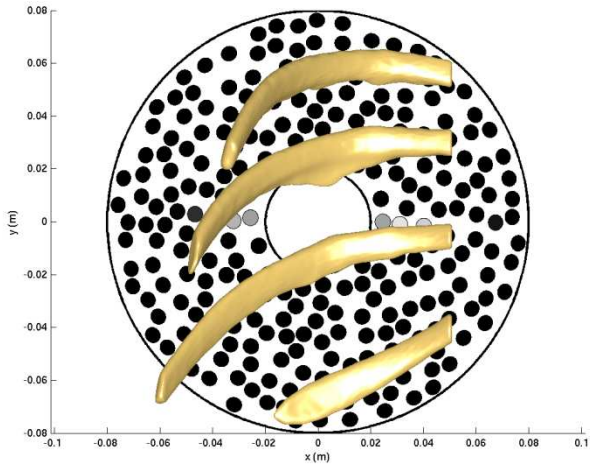

Figure 2. Position of ribs with respect to HIFU array looking in the negative z direction.

From a knowledge of $[H]^{-1}[\beta]$, the acoustic pressure on the surface of the ribs may be obtained using equation (9) for a given distribution of source velocities. In order to formulate the cost function and the constraints, the case of all elements vibrating in phase and with unit velocity amplitude was investigated. The incident acoustic pressure field at selected locations in the *y*-*z* plane in absence of ribs is shown in figure 3. The corresponding acoustic pressure field in the medium with the ribs present is shown in figure 4.

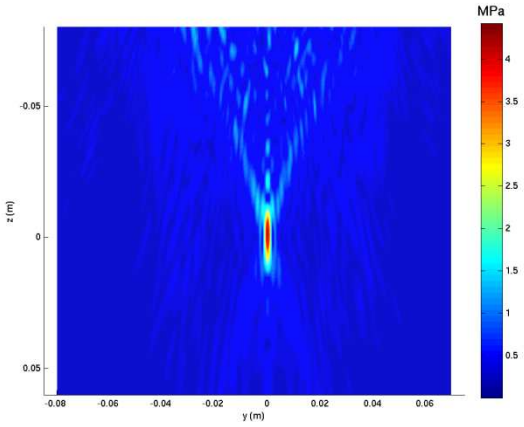

Figure 3. Incident acoustic pressure magnitude in *y*-*z* plane resulting from field of 1 MHz multi-element array. Uniform unit amplitude velocity and zero phase.

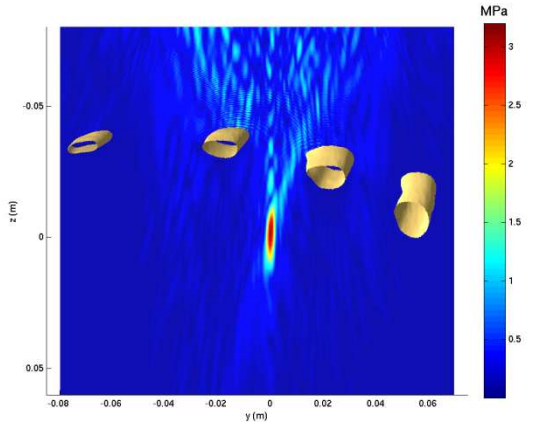

Figure 4. Acoustic pressure magnitude in *y*-*z* plane resulting from field of 1 MHz multi-element array. Uniform unit amplitude velocity and zero phase. Contour of ribs shown in bone colour.

The resulting acoustic dose rate on the surface of the ribs is shown in figure 5: this is shown in a plan view looking in the positive *z*-direction since the ribs are three-dimensional and their surface does not form a plane.

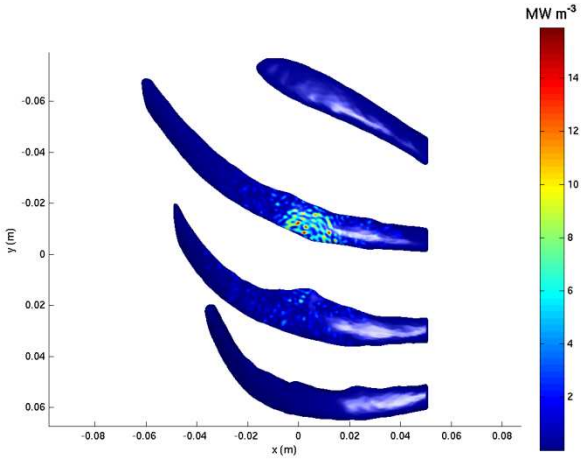

Figure 5. Acoustic dose rate on surface of ribs resulting from field of 1 MHz multi-element array. Spherical focusing (uniform unit amplitude velocity and zero phase).

Figures 3 and 4 show that inserting the ribs between the array and the focus causes the acoustic pressure magnitude at the focus to drop from 4.4 MPa to 3.2 MPa. Figure 5 shows that the maximum acoustic dose rate value on the surface of the ribs is 16 MW m^{-3} (corresponding to an acoustic pressure of 1.6 MPa) for the spherical focusing case, with all elements of the array vibrating at an amplitude of 1 m s^{-1} and with uniform phase.

The NAG Numerical Library *e04us* routine was used to carry out the constrained minimisation [15]. It is designed to minimise an arbitrary smooth sum of squares function subject to constraints, which may include simple bounds on the variables, linear constraints and smooth nonlinear constraints. The procedure is described further in [12].

To fulfil the chosen requirement of a reduction to 30% in the rib surface acoustic dose rate compared to the spherical focusing case, the value $p_{surf_{max}}$ used to compute the acoustic dose rate in equation (17) was set to 0.88 MPa. U_{max} was selected to be 1 m s^{-1}. The vector of pressures in the exterior volume featured in the cost function (i.e. the 'desired' field pressure distribution) was generated from pressure field values in absence of ribs at 9261 equally spaced locations in a 21×21×21 cubic Cartesian grid such that -1.5 cm ≤ x ≤ 1.5 cm, -1.5 cm ≤ y ≤ 1.5 cm and -1.5 cm ≤ z ≤ 1.5 cm, the focus of the array being at the global origin.

The surface mesh of the ribs contains 200921 nodes. It is both impractical and unnecessary to impose a constraint at all these locations on the surface of the scatterer. Too high a number of constraints may result in numerical instability and some locations on the surface of the ribs are highly unlikely to exceed $p_{surf_{max}}$, in particular those not directly facing the array. Hence, surface locations associated with pressure magnitudes below 40% of the maximum pressure correspond to the acoustic dose rate quantity in figure 5 (i.e. locations on the rib surface where the pressure was less than 0.64 MPa) were not included in the constraints. This resulted in only 3390 constraints associated with the pressure magnitude on the ribs being required, along with the 256 constraints for the magnitude of the element velocities. It will be verified after the optimisation that all nodes on the surface of the ribs are below the chosen pressure magnitude threshold.

With the above input conditions, a solution was obtained. The real and imaginary parts of the velocities were subsequently rescaled and the surface and field pressures calculated. Figures 6a and 6b respectively display the magnitudes and phases of the element velocities of the array resulting from the constrained minimisation. It was verified that the velocity magnitudes did not exceed 1 m s^{-1}.

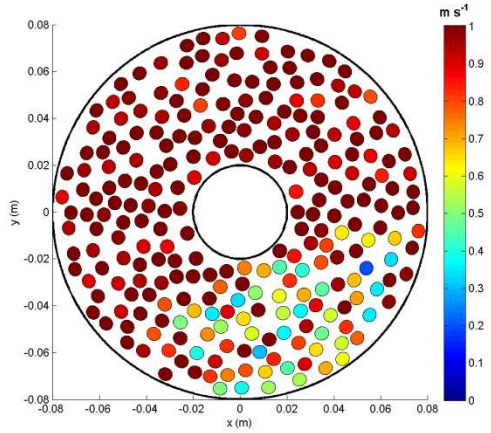

Figure 6a. Source velocity magnitudes resulting from constrained minimisation.

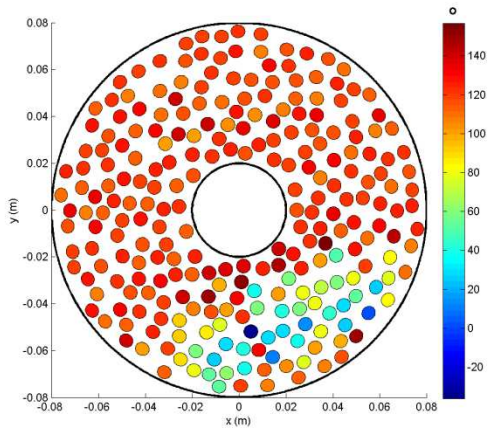

Figure 6b. Source velocity phases resulting from constrained minimisation.

Figure 7 shows the acoustic pressure magnitude in the y-z plane resulting from the source velocity distribution displayed in figures 6a and 6b.

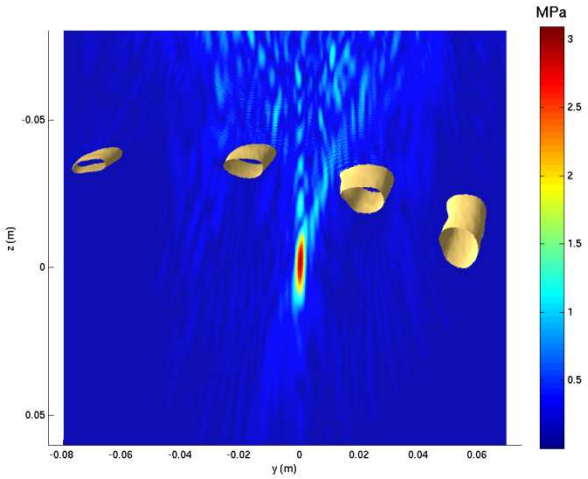

Figure 7. Acoustic pressure magnitude in *y*-*z* plane resulting from field of 1 MHz multi-element array. Source velocity distribution obtained from constrained minimisation.

Figure 7 shows that an overall reduction in the back-scattered acoustic pressure is achieved as a consequence of the constrained minimisation, when compared against the uniform amplitude and phase results displayed in figure 4. Although the constrained minimisation algorithm is unsuccessful at rendering a peak pressure of 4.4 MPa which was obtained in the absence of ribs (Figure 3), it is now 3.1 MPa, only 3% lower than in the case of spherical focusing in the presence of ribs (Figure 4).

Figure 8 shows the acoustic dose rate on the surface of the ribs, resulting from the source velocity distribution displayed in figures 6a and 6b.

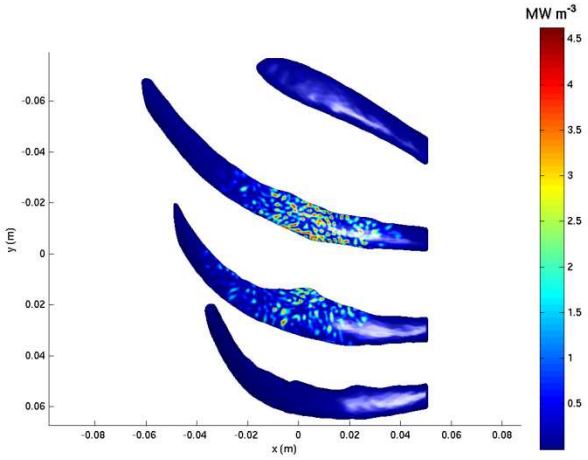

Figure 8. Acoustic dose rate on surface of ribs resulting from field of 1 MHz multi-element array. Source velocity distribution obtained from constrained minimisation.

The maximum acoustic dose rate on the bone side of the surface of the ribs is now 4.7 MW m^{-3}, corresponding to a maximum acoustic pressure of 0.88 MPa. A reduction in the maximum rib surface

acoustic dose rate to 30% is therefore achieved with an ensued reduction in peak focal pressure compared with the spherical focusing case of only 3%.

4. Conclusions

An approach based on a GMRES implementation of the Helmholtz integral equation boundary element formulation was validated to model the scattering of the field of a multi-element random HIFU phased array by ribs of an arbitrary geometry under continuous wave excitation. The medium surrounding the scatterer featured a complex speed of sound thus allowing a phenomenological approach to modelling absorption effects. A surface acoustic impedance boundary condition was implemented to account for the fact that the ribs are not perfectly rigid and will also absorb acoustic energy. This enabled the calculation of an acoustic dose rate parameter on the surface of the ribs defined as the time-averaged relaxational absorption per unit volume [13].

Using the discretised form of the Helmholtz integral equation for locations in the exterior volume and on the surface of the scatterer, the inverse problem of determining the complex velocities of a multi-element array which produces an acoustic pressure field that best fits a required acoustic pressure distribution in a least-squares sense was formulated such that:

- The acoustic dose rate on the surface of the scatterer did not exceed a specified threshold, defined as 30% of the maximum acoustic dose rate resulting from spherical focusing.
- The amplitude of the velocity of each element on the array was bounded by maximum value specified as 1 m s^{-1}.

This approach was tested on a 1 MHz 256-element spherical array in presence of anatomical ribs. Employing a NAG library solver, a least-squares minimisation with nonlinear constraints was carried out to solve the above problem, where the gradients of the objective function and of the constraints with respect to the optimisation variables were provided. The solver returned a set of real and imaginary parts for the source velocities which satisfied both sets of constraints, hence reducing the back-scatterered pressure from the ribs and the acoustic dose rate on the surface of the scatterer compared with the spherical focusing case.

Further validation of the constrained minimisation methodology on other rib topologies is currently underway. The technique is also being benchmarked against binarised apodisation based on ray tracing and against the DORT method. This will form the topic of a future publication.

Acknowledgements

The authors would like to acknowledge the support of the National Measurement Systems Directorate of the UK Department of Business, Innovation and Skills and EPSRC EP/F025750/1. This work was supported in parts by the European Metrology Research Programme (Joint Research Project HLT03, which is jointly funded by the EMRP participating countries within EURAMET and the European Union) and by the Acoustics and Ionizing Radiation programme of the UK National Measurement Office. The authors are grateful to PACSYS Ltd. for supplying stand-alone executables of the Program for Automatic Finite Element Calculations boundary element routines as well as for useful discussions. The authors would equally like thank Minh Hoang for advice on inverse methods and help with NAG Numerical Library solvers. The authors would like to acknowledge the support of Tristan Clarke for IT-related matters. They would also like to express their gratitude to David Sinden, Ian Rivens, Simon Arridge and Timo Betcke for useful discussions

References

[1] Gélat P, ter Haar G and Saffari N 2011 Modelling of the acoustic field of a multi-element HIFU array scatterred by human ribs *Phys. Med. Biol.* **56** 5553.

[2] Crum L, Bailey M, Hwang J H, Khokhlova V and Sapozhnikov 2010 Therapeutic ultrasound: Recent trends and future perspectives *Physics Procedia* **3** 25

[3] Leslie T, Ritchie R, Illing R, ter Haar G, Phillips R, Middleton M, Wu F and Cranston D 2012 High-intensity focused ultrasound treatment of liver tumours: post-treatment MRI correlates

well with intra-operative estimates of treatment volume *Brit. J. Radiol.* **85** 1363–1370.
[4] Wu F, Zhi-Biao W, Wen-Zhi C, Hui Z, Jin B, Jian-Zhong Z, Ke-Quan L, Cheng-Bing J, Fang-Lin X, Hai-Bing S 2004 Extracorporeal high intensity focused ultrasound ablation in the treatment of patients with large hepatocellular carcinoma *Ann. Surg. Oncol*. **11** 1061
[5] Li J-L, X-Zh Liu, Zhang D, Gong X-F 2007 Influence of ribs on nonlinear sound field of therapeutic ultrasound. *Ultrasound Med. Biol.* **33** 1413
[6] Liu H-L, Chang Hsu, Chen W-S, Shih T-C, Hsiao J-K and Lin W-L. Feasibility of transrib focused ultrasound thermal ablation for liver tumours using a spherically curved 2D array: A numerical study 2007 *Med. Phys.* **34** 3436
[7] Quesson B, Merle M, Roujol S, de Senneville B D and Moonen C T. A method for MRI guidance of intercostal high intensity focused ultrasound ablation in the liver 2010 *Med. Phys.* **37** 2533
[8] Marquet F, Aubry J F, Pernot M, Fink M and M Tanter. Optimal transcostal high-intensity focused ultrasound with combined real-time 3D movement tracking and correction 2011 *Phys. Med. Biol.* **56** 7061
[9] Prada C, 2002 Detection and imaging in complex media with the DORT method *Top. Appl. Phys.* **84**, 107
[10] Cochard E, Aubry J-F, Tanter M and Prada C 2011 Adaptive projection method applied to three-dimensional ultrasonic focusing and steering through the ribs *J. Acoust. Soc. Am.* **130** 716
[11] Ballard J, Casper A J, Wan Y and Ebbini E S 2010 Adaptive Transthoracic Refocusing of Dual-Mode Ultrasound Arrays *IEEE T. Bio-med. Eng.* **57** 93
[12] Gélat P, ter Haar G and Saffari N 2012 The optimisation of acoustic fields for ablative therapies of tumours in the upper abdomen *Phys. Med. Biol.* **57** 8471.
[13] Duck F A 2009 Acoustic dose and acoustic dose rate *Ultrasound Med. Biol.* **35** 1679
[14] Nyborg W L 1981 Heat generation by ultrasound in a relaxing medium *J. Acoust. Soc. Am.* **70** 310
[15] http://www.nag.co.uk/numeric/numerical_libraries.asp
[16] Courant R and Hilbert D 1962 *Methods of Mathematical Physics* Vol. 2 (New York: Interscience; 1962), p258
[17] Colton D and Kress R 1983 Integral Equation Methods in Scattering Theory (Pure and Applied Mathematics) (New York: Wiley), p81 and p84
[18] Morse P M and Ingard K U 1968 *Theoretical Acoustics* (New York: McGraw-Hill), p422
[19] Wein W, Brunke S, Khamene A, Callstrom M R and Navab N 2008 Automatic CT-ultrasound registration for diagnostic imaging and image-guided intervention *Med. Image Anal.* **12** 577
[20] El-Brawany M A, Nassiri D K, Ter Haar G, Shaw A, Rivens I and Lozhken K 2009 Measurement of thermal and ultrasonic properties of some biological tissues *J. Med. Eng. Technol.* **33** 249.